Highly efficient nonlinear energy sink

Mohammad AL-Shudeifat

Highly efficient nonlinear energy sink

Mohammad A. AL-Shudeifat

Abstract The performance of the nonlinear energy sink (NES) that composed of a small mass and essentially nonlinear coupling stiffness with a linear structure is considerably enhanced here by including the negative linear and nonlinear coupling stiffness components. These negative linear and nonlinear stiffness components in the NES are realized here through the geometric nonlinearity of the transverse linear springs. By considering these components in the NES, very intersecting results for passive targeted energy transfer (TET) are obtained. The performance of this modified NES is found here to be much improved than that of all existing NESs studied up to date in the literature. Moreover, nearly 99 % of the input shock energy induced by impulse into the linear structures considered here has been found to be rapidly transferred and locally dissipated by the modified NES. In addition, this modified NES maintains its high performance of shock mitigation in a broadband fashion of the input initial energies where it keeps its high performance even for sever input energies. This is found to be achieved by an immediate cascade of several resonance captures at low- and high- nonlinear normal modes frequencies. The findings obtained here by including the negative linear and nonlinear stiffness components are expected to significantly enrich the application of these stiffness components in the TET field of such nonlinear oscillators.

Keywords Nonlinear oscillation · Nonlinear energy sink · Targeted energy transfer · Nonlinear stiffness · Negative stiffness · Passive energy pumping

M. A. AL-Shudeifat (✉)
Aerospace Engineering, Khalifa University of Science, Technology & Research, P.O. Box 127788, Abu Dhabi, UAE
e-mail: mohd.shudeifat@kustar.ac.ae

List of symbols

NES	Nonlinear energy sink
TET	Targeted energy transfer
NNMs	Nonlinear normal modes
SSVI	Single-sided vibro-impact
L	Spring physical unloaded length
L_0	Spring compressed length
Δ	Deflection in the spring
F_{nl}	Springs exact nonlinear force
$\tilde{F}_{\text{nl}}$	Taylor approximation of F_{nl}
m	Nonlinear energy sink mass
k	Transverse spring linear stiffness
k_{nl}	Spring geometric nonlinear stiffness
λ	Nonlinear energy sink linear damping coefficient
λ_{p}	Primary mass linear damping coefficient

1 Introduction

Shock mitigation in small- and large-scale dynamic structures using nonlinear energy sinks (NESs) has

gained considerable interest in the past decade. Accordingly, an extensive research work has been done for investigating the targeted energy transfer through different designs of NESs. The NES is single or two-degree-of-freedom light-weighted device coupled to small- or large-scale dynamic structure through essentially nonlinear elements [1–14]. It performs rapid and passive energy transfer and dissipation for significant portion of the vibration energy induced by impulse into the linear primary structure (due to shock, blast, earthquakes, etc.). Purely cubic springs have been employed in Type I, Type II, and Type III NESs where no negative or positive linear stiffness components were considered in these designs [1–11]. Type I NES is composed of a small mass coupled to the linear structure through linear damping and essentially nonlinear stiffness elements where the Type II NES is coupled to the linear structure through both nonlinear stiffness and nonlinear damping elements. The Type III NES is composed of two masses where the upper NES mass is coupled to the bottom one through essentially nonlinear stiffness element, whereas the bottom NES mass is also coupled to the linear structure through essentially nonlinear stiffness element [10].

The strongly nonlinear inertia coupling in the rotating NES device which couples the rotating NES mass to the linear structure has been investigated in [12–14] where good performance of this NES for shock mitigation was observed. The strongly nonlinear vibro-impact coupling between the NES mass and the linear structure at the degree of freedom that exhibits high vibration amplitudes has also been investigated in [15–20] as an efficient NES design. Recently, the most efficient single-sided vibro-impact (SSVI) NES was numerically and experimentally studied in [20]. Unlike other designs, The SSVI design was found to be efficient in shock mitigation even at severe initial input energies induced into the linear structure. Moreover, a set of SSVI NESs have been employed via synergy with Type I NESs with a 9-story test structure excited by a blast where the SSVI NESs have been found to have the main contribution for energy scattering to high modes which yields rapid and strong mitigation of the blast shock [21].

In all NESs, the basic mechanism for the TET takes place through single mode or cascade of modes resonance captures [1–8,12–14,20–23]. The NES performance for rapid passive energy transfer from the linear structure to the NES itself can be quantified through the percentage of the initial energy induced into the linear structure that is transferred and rapidly dissipated by the NES. Furthermore, effective measures for damping and stiffness have been introduced for studying the effect of the NES attachment on enhancing the damping and the stiffness of the linear structure [9,20,22,23]. As a result, the performance of the NES attachment was also accurately quantified through these measures.

In all above NESs, the NES mass is coupled to the linear structure through essentially nonlinear element. However, a completely different configuration of another NES design has been investigated in [24,25] for studying the steady-state dynamics of a linear structure subjected to harmonic excitation. In this design, one side of the NES mass was weakly coupled to the linear structure by a linear spring, and the other side was grounded to the wall by an essentially nonlinear stiffness. Even though the authors in [24] have claimed that passive energy pumping has been achieved, the authors in [25] have claimed that no evidence of energy pumping was observed by considering similar system of similar physical parameters.

The physical configuration of Type I NES used in the literature in [1–11,21–23] can be modified to generate negative linear and nonlinear stiffness components. This modification is the main focus in this paper where the significant effect of the negative stiffness components in enhancing the TET in the NES is clearly addressed here. This bistable NES with the negative stiffness components has two stable equilibrium positions. Selecting one of these equilibrium positions to coincide with the equilibrium position of the coupling mass in the linear structure is the key behind the considerable enhancement in the NES performance for rapid passive energy transfer and dissipation in broadband fashion of input energies. In addition, significant finding is observed when the bistable NES attachment with negative linear and nonlinear stiffness components has a nonzero relative displacement relative to the linear primary structure away from the NES equilibrium positions. This leads to a strong suppression of the vibration amplitudes of the linear structure in the first cycle of oscillation for wide range of initial input energies induced into the linear structure. The enhanced NES design here through including small negative linear and nonlinear stiffness components is highly efficient design compared with all existing NESs investigated up to date in the related literature.

2 Realizing negative linear and nonlinear stiffness components in the NES

The configuration in Fig. 1 has been used in [8] for realizing the essentially nonlinear stiffness based on the geometric nonlinearity obtained by the transverse linear springs when they are not compressed or elongated at their vertical position. Hence, the resulting essentially nonlinear oscillator has no linear stiffness components. Here we assume that these transverse springs are compressed when they are aligned in their vertical position where an amount of potential energy is stored. This can be achieved by considering the bistable geometry in Fig. 1a which has two stable equilibrium positions at which both springs are not stretched or compressed. This configuration of the unloaded springs generates negative linear and nonlinear stiffness components during the motion of the mass. The two stable equilibrium positions of the NES mass (no tension or compression in the springs at their physical length L) are at $z = 0$ and $z = 2z_c$ for $z_c > 0$ relative to the selected reference of the displacement as shown in the figure. Consequently, the configuration of the NES is unstable at $z = z_c$. For the following analysis, the initial position of the mass m is selected to coincide with the left equilibrium position of the system (i.e., $z = 0$). Consequently, the net horizontal force F_{nl} of the springs becomes zero when the mass at the positions $z = 0$, $z = z_c$, and $z = 2z_c$. However, the net vertical force of the springs is always equal to zero due to the symmetry.

The realization to the negative linear and nonlinear stiffness components in the system is verified by deriving the relation of the net horizontal force $F_{nl}$of the springs based on the geometry in Fig. 1b after the mass moves to the right by the displacement z. Hence, for the deflection $\Delta = -L + (L_0^2 + (-z_c)^2)^{1/2})$ of each spring, the net nonlinear force of the springs acting on the mass is derived as

$$F_{nl} = -2k\,(z - z_c)\left(\frac{\left(L_0^2 + (z - z_c)^2\right)^{1/2} - L}{\left(L_0^2 + (z - z_c)^2\right)^{1/2}}\right) = -2k\,(z - z_c)\left(1 - L\left(L_0^2 + (z - z_c)^2\right)^{-1/2}\right), \quad (1)$$

where $L = (L_0^2 + z_c^2)^{1/2}$ which is the unloaded spring physical length. The Taylor-expansion about $z = z_c$ for the quantity $(L_0^2 + (z - z_c)^2)^{-1/2}$ yields

$$\left(L_0^2 + (z - z_c)^2\right)^{-1/2} = \frac{1}{L_0} - \frac{(z - z_c)^2}{2L_0^3} + \frac{3\,(z - z_c)^4}{8L_0^5} - \frac{5\,(z - z_c)^6}{16L_0^7} + O\left((z - z_c)^8\right). \quad (2)$$

By substituting Eq. (2) into (1) for $\bar{z} = z - z_c$we obtain

$$F_{nl} \cong \tilde{F}_{nl} = -2k\left(1 - \frac{L}{L_0}\right)\bar{z} - \frac{kL}{L_0^3}\bar{z}^3 + \frac{3kL}{4L_0^5}\bar{z}^5 - \frac{5kL}{8L_0^7}\bar{z}^7 + O\left(\bar{z}^9\right) = k_1\bar{z} - k_2\bar{z}^3 + k_3\bar{z}^5 - k_4\bar{z}^7 + O\left(\bar{z}^9\right), \quad L_0 < L, \quad (3)$$

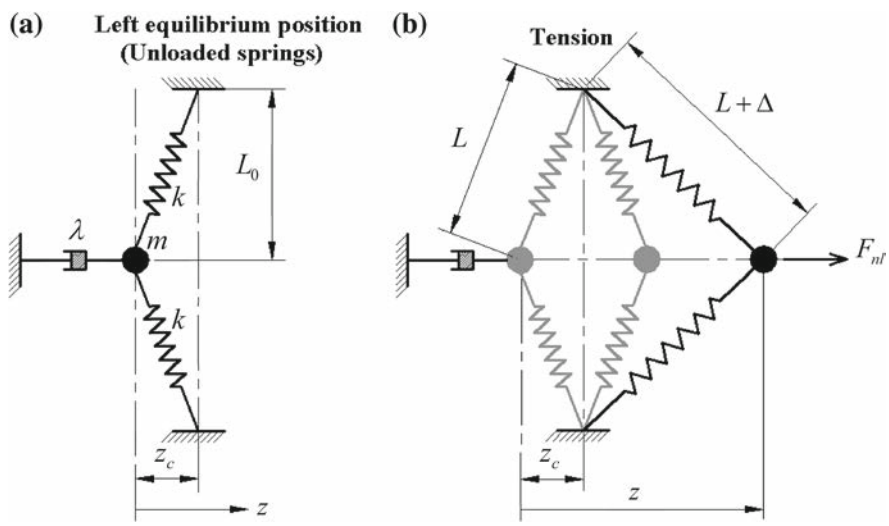

Fig. 1 Physical configuration of the nonlinear damped oscillator

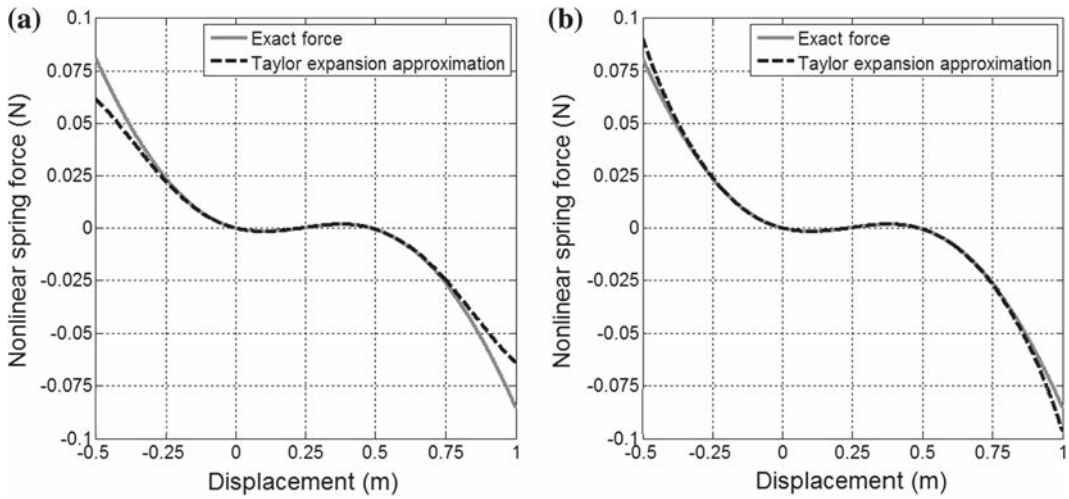

Fig. 2 Exact nonlinear forces of the springs obtained by Eq. (1) and their corresponding approximated forces obtained by Eq. (3) for $k_4 = 0$ in **a** and $k_4 \neq 0$ in **b**

where $k_1 = 2k\left(\frac{L}{L_0} - 1\right)$, $k_2 = \frac{kL}{L_0^3}$ $k_3 = \frac{3kL}{4L_0^5}$ and $k_4 = \frac{5kL}{8L_0^7}$ for $L_0 < L$.

For the arbitrary parameters of $k = 0.3$ N/m, $L_0 = 0.97$ m, and $L = 1$ m, the results in Fig. 2 for the exact nonlinear force F_{nl} in Eq. (1) and its corresponding approximated nonlinear force $\tilde{F}_{\text{nl}}$ in Eq. (3) of the springs in Fig. 1 show the significance of including the seventh order nonlinear stiffness coefficients, because later we will see that the mass m is expected to exhibit high amplitudes of oscillation when the system in Fig. 1 is used as a nonlinear energy sink for passive energy transfer and dissipation.

3 Application for passive energy pumping

The nonlinear attachment in Fig. 1a of mass m is now attached to the single-degree-of freedom linear dynamic oscillator of mass $M (m \ll M)$ as shown in Fig. 3. The purpose of that is to investigate the passive energy transfer from this linear structure to the modified NES attachment. The equilibrium position of the linear structure is selected to coincide with the left stable equilibrium position of the attachment at which springs are neither compressed nor elongated. This configuration shows that an amount of potential energy will be stored

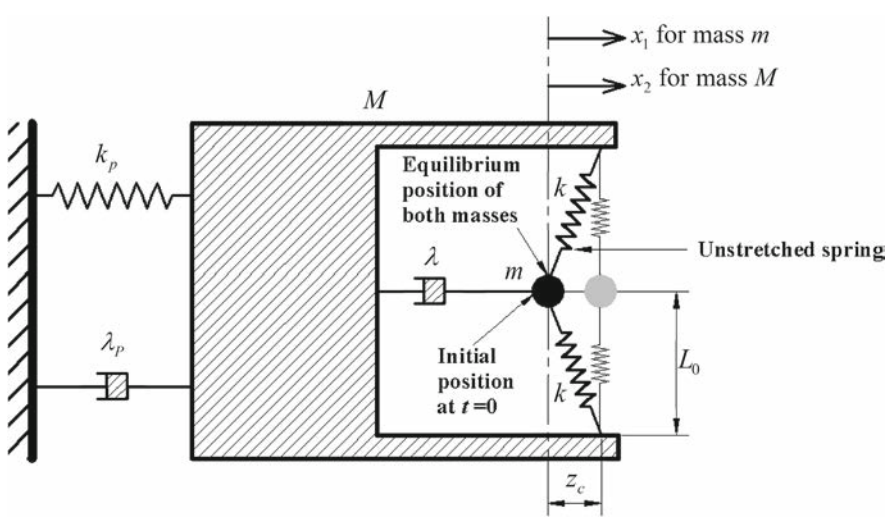

Fig. 3 Single-degree-of-freedom linear structure coupled to the modified NES

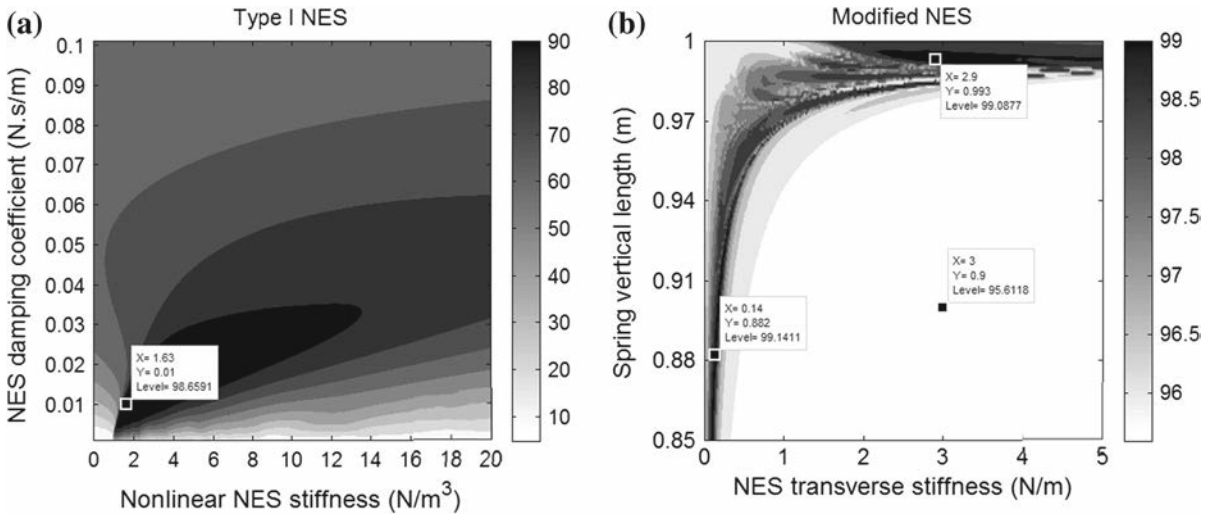

Fig. 4 Percentage of the initial energy induced into the primary mass dissipated by the NESs (*colored bar*) for various stiffness and damping coefficients of the Type I NES in **a** and various stiffness coefficients and spring vertical lengths of the modified NES in **b**

in the NES mass when the linear transverse springs are aligned at their vertical position.

For the relative displacement between the NES mass and the linear structure mass $z = x_1 - x_2$ and $z_c > 0$ the equations of motion are given as

$$\begin{aligned} &m\ddot{x}_1 + \lambda\,(\dot{x}_1 - \dot{x}_2) - k_1(z - z_c) + k_2\,(z - z_c)^3 \\ &\quad -k_3\,(z - z_c)^5 + k_4\,(z - z_c)^7 = 0, \\ &M\ddot{x}_2 + \lambda_p\dot{x}_2 - \lambda\,(\dot{x}_1 - \dot{x}_2) + k_p x_2 + k_1(z - z_c) \\ &\quad -k_2\,(z-z_c)^3 + k_3\,(z-z_c)^5 - k_4\,(z-z_c)^7 = 0, \end{aligned} \tag{4}$$

where x_1 is the NES mass displacement, x_2 is linear structure mass displacement, λ is the damping of the NES attachment, λ_P is the damping of the linear structure, and k_p is the stiffness of the linear structure.

3.1 Initially unloaded springs

Series of simulations for the system in Fig. 3 are performed here to compare the performance of the modified NES in Fig. 3 to the existing Type I NES in the literature [1–11,21–23] obtained by setting $L = L_0$. The primary linear structure in Fig. 3 is assumed to have the parameters $M = 1$ kg, $k_p = 1$ N/m, and $\lambda_p = 0.001$ N s/m. Both Type I and the modified NESs are assumed to have the same mass of $m = 0.05$ kg and the unloaded spring length of $L = 1$ m. The NES performance is quantified by the percentage of the initial input energy induced into the linear structure that is passively transferred and dissipated by the NES where this percentage is represented by η. Based on η, the damping and the nonlinear stiffness coefficients of Type I NES ($L = L_0, z_c = 0$) are optimized in Fig. 4a at $\dot{x}_2(0) = 0.1$ m/s to be $\lambda = 0.01$ N s/m and $k_{nl} = 1.63$ N/m^3 at $\eta = 98.7$ %.

The Type I NES is now modified by the configuration in Fig. 3 for which $L > L_0$ and $z_c > 0$ and optimized at the same optimized damping $\lambda = 0.01$ N s/m obtained previously for Type I NES. Hence, at $\dot{x}_2(0) = 0.1$ m/s we obtain two sets of the optimized values of k and L_0 for which $\eta > 99$ % as shown in Fig. 4b. These sets are shown in this figure at $\eta = 99.14$ % to be $k = 0.14$ N/m and $L_0 = 0.882L$ and at $\eta = 99.09$ % to be $k = 2.9$ N/m and $L_0 = 0.993L$. The performance of the modified NES at these two sets of the optimized parameters is compared with that of the optimized Type I NES for wide range of initial input energies induced into the linear structure mass, which are represented by their corresponding initial velocities as shown in Fig. 5. It is clear from the figure that for $k = 0.14$ N/m and $L_0 = 0.882L$ of the modified NES the performance is within the range $97\ \% < \eta < 99\ \%$ for wide range of input energies. This performance is considerably enhanced here compared with that of Type I NES as shown in the same figure. For 100 s of simulation the modified NES at $k = 0.14$ N/m and $L_0 = 0.882L$ keeps its high performance as shown in Fig. 6 while

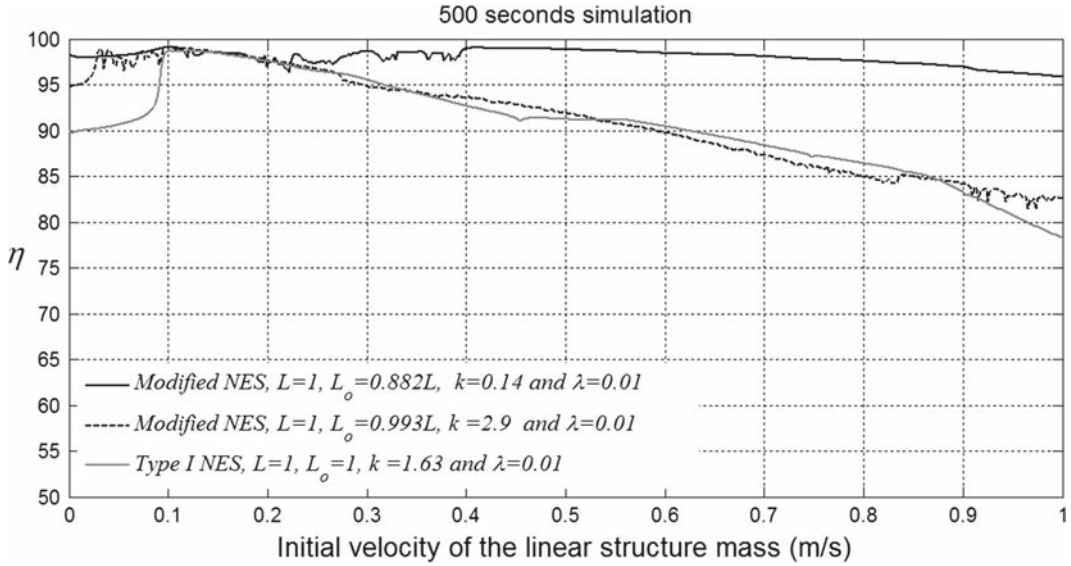

Fig. 5 Percentage of the initial energy induced into the primary mass dissipated by the Type I NES and the modified NESs for various initial velocities of the primary mass

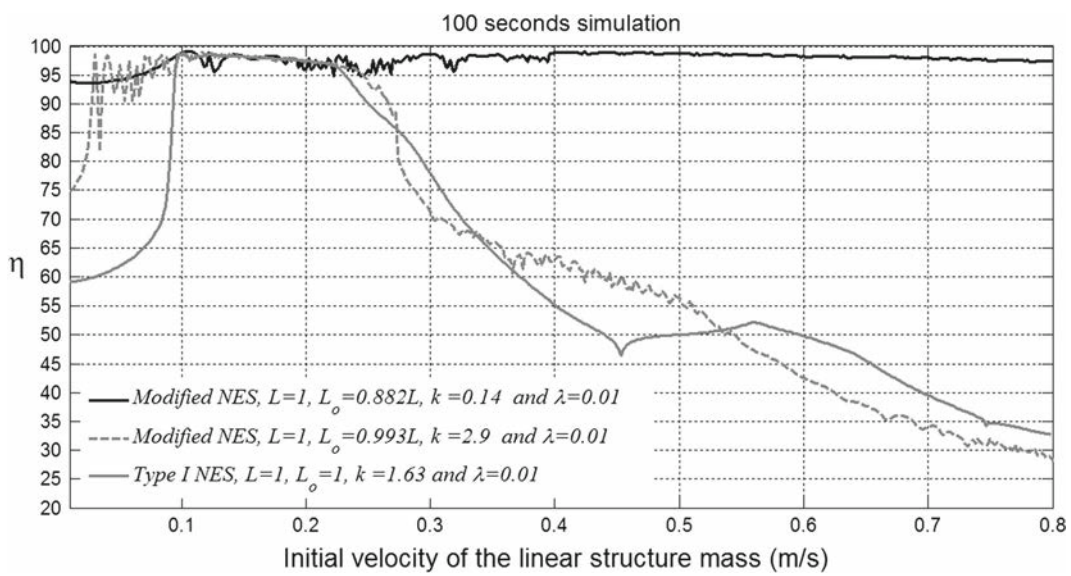

Fig. 6 Percentage of the initial energy induced into the primary mass dissipated by the Type I NES and the modified NESs for various initial velocities of the primary mass

the optimized Type I NES shows poor performance for significant ranges of the input energies. The other optimized set of the modified NES at $k = 2.9$ N/m and $L_0 = 0.993L$ has a performance close to Type I, since $L_0 \cong L$ which makes it behaves closely to Type I NES as shown in Figs. 5 and 6.

Considering the optimized modified NES at $k = 0.14$ N/m, $\lambda = 0.01$ N s/m, and $L_0 = 0.882L$ and the optimized Type I NES at $\lambda = 0.01$ N s/m and $k_{nl} = 1.63$ N/m^3, the time histories and their corresponding wavelet transforms of the displacement of the linear structure mass and the relative displacement of the NES mass are plotted in Figs. 7, 8, 9, 10 for different input energies. Both Type I NES in Fig. 7 and the modified NES in Fig. 8 show high performance in energy transfer and dissipation for $\dot{x}_2(0) = 0.1$ m/s

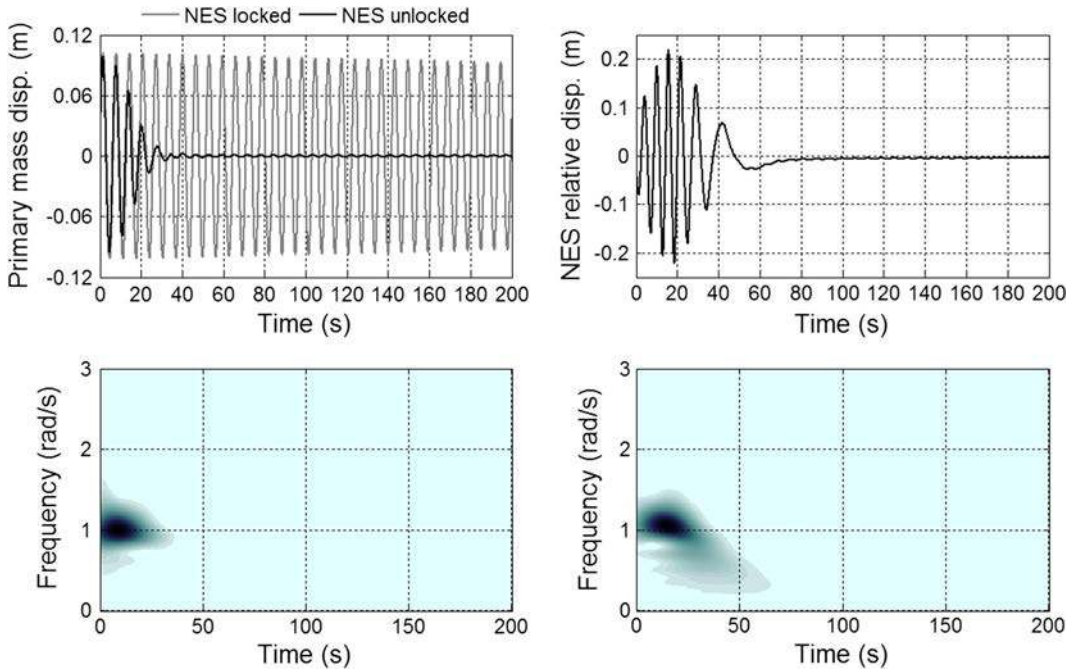

Fig. 7 Time histories of the displacement of the primary mass and the relative displacement of the optimized Type I NES mass and their corresponding wavelet transforms for $\dot{x}_2\,(0) = 0.1$ m/s

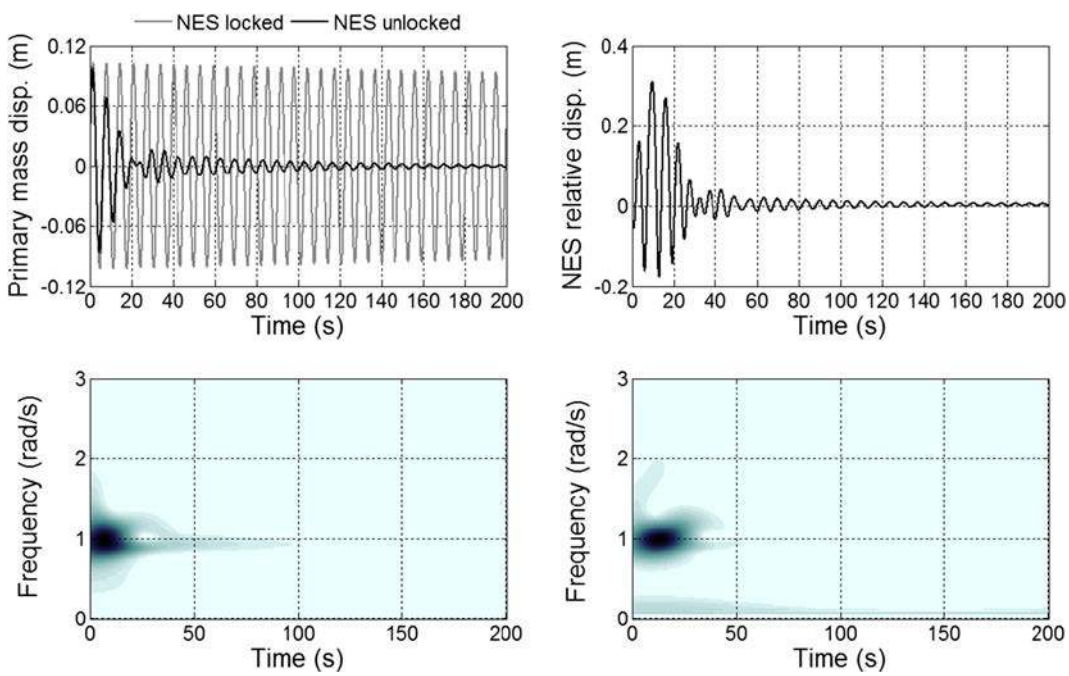

Fig. 8 Time histories of the displacement of the primary mass and the relative displacement of the optimized modified NES mass and their corresponding wavelet transforms for $\dot{x}_2\,(0) = 0.1$ m/s

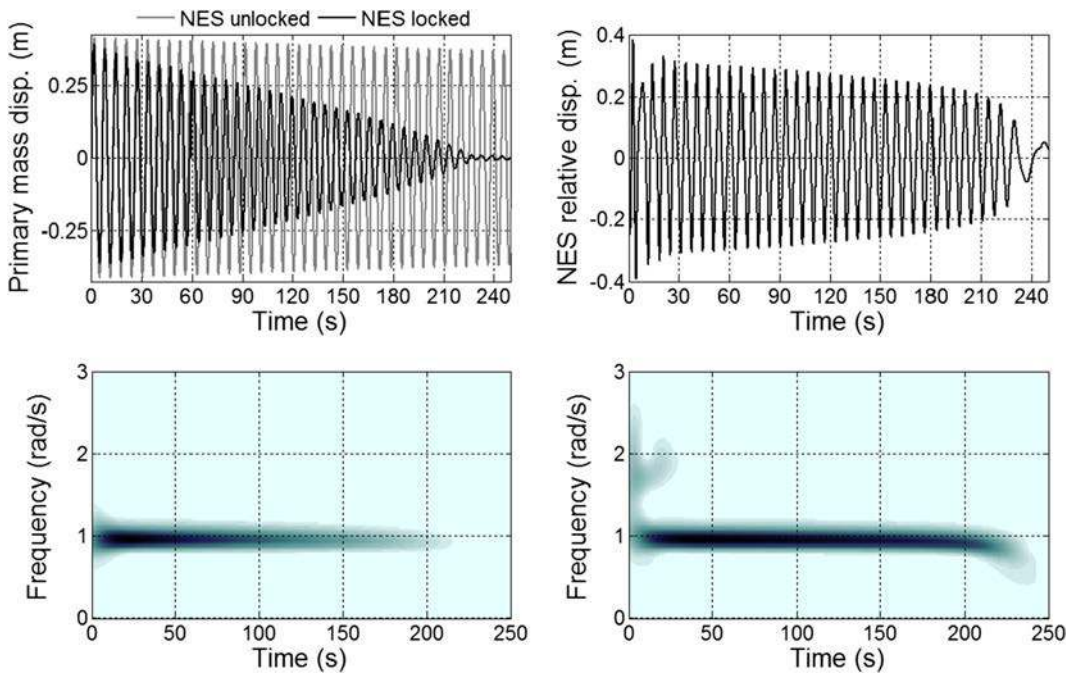

Fig. 9 Time histories of the displacement of the primary mass and the relative displacement of the optimized Type I NES mass and their corresponding wavelet transforms for $\dot{x}_2\,(0) = 0.4$ m/s

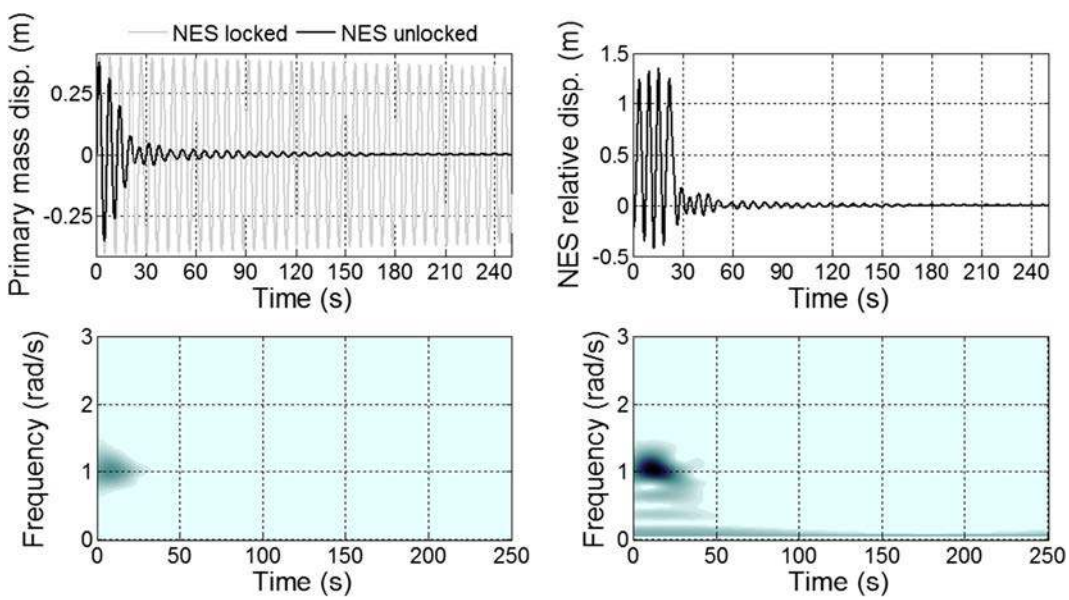

Fig. 10 Time histories of the displacement of the primary mass and the relative displacement of the optimized modified NES mass and their corresponding wavelet transforms for $\dot{x}_2\,(0) = 0.4$ m/s

where the responses are strongly dominated by 1:1 resonance capture as shown in the corresponding wavelet transforms. However, for $\dot{x}_2\,(0) = 0.4$ m/s the response of the Type I NES in Fig. 9 shows considerably less performance than the modified NES shown Fig. 10. The corresponding wavelet transform of the Type I NES

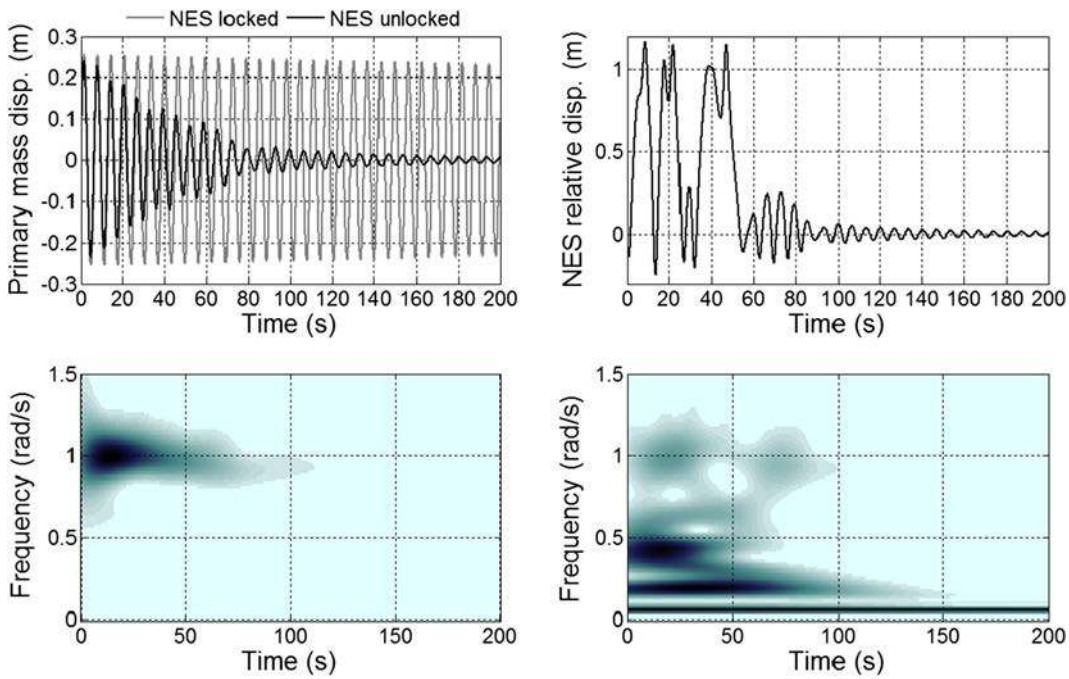

Fig. 11 Time histories of the displacement of the primary mass and the relative displacement of the optimized modified NES mass and their corresponding wavelet transforms for $\dot{x}_2\,(0) = 0.25$ m/s

response in Fig. 9 is strongly dominated by the 1:1 resonance capture. However, the response of the modified NES in Fig. 10 is dominated by a cascade of immediate resonance captures at the 1:1 NNM branch besides to a set of NNM branches of low frequencies as shown in the corresponding wavelet transform of the modified NES relative displacement. This energy scattering by an immediate cascade of resonance captures makes the modified NES to be capable to keep its high performance in shock mitigation at high initial input energy.

Furthermore, to verify the observed cascade of resonance captures by the modified NES, the time histories of the displacements and their corresponding wavelet transforms are obtained at an intermediate input energy of $\dot{x}_2\,(0) = 0.25$ m/s in Fig. 11 and at high input energy of $\dot{x}_2\,(0) = 0.7$ m/s in Fig. 12. It is clear in these figures that the modified NES keeps its strong and immediate cascade of resonance capture at 1:1 NNM branch and the NNM branches of low frequencies. However, at the high input energy in Fig. 12, the modified NES has an additional strong resonance capture by higher NNM frequency branch.

The actual nonlinear forces in the NESs are plotted in Fig. 13 based on the simulation results for the Type I NES and the modified one at the initial velocities of the primary mass of $\dot{x}_2\,(0) = 0.1$ m/s,$\dot{x}_2\,(0) = 0.25$ m/s, $\dot{x}_2\,(0) = 0.4$ m/s, and $\dot{x}_2\,(0) = 0.7$ m/s. For low initial energy corresponding to $\dot{x}_2\,(0) = 0.1$ m/s, the modified NES oscillates about its left equilibrium position as shown in Fig. 13a where the strong nonlinearity in the left branch of the force is clearly shown. For higher initial energies corresponding to the initial velocities in Fig. 13b, c, d, the modified NES exchanges oscillation between its left and right equilibrium positions. The oscillation through the two equilibrium positions gives the NES mass larger strokes (peak-to-peak amplitudes) of oscillation by which much more energy is dissipated by the modified NES than Type I NES. Unlike the modified NES, it is shown in the figure that the motion of the Type I NES is restricted by narrow strokes (peak-to-peak amplitudes) of oscillations at the intermediate and the high loads which restrict the amount of the energy transferred and dissipated by the NES.

The effect of the change in the modified NES damping and stiffness values is investigated in Fig. 14a for $\dot{x}_2\,(0) = 0.1$ m/s and in Fig. 14b for $\dot{x}_2\,(0) = 0.4$ m/s. It is found that, unlike Type I NES in Fig. 4a, the perfor-

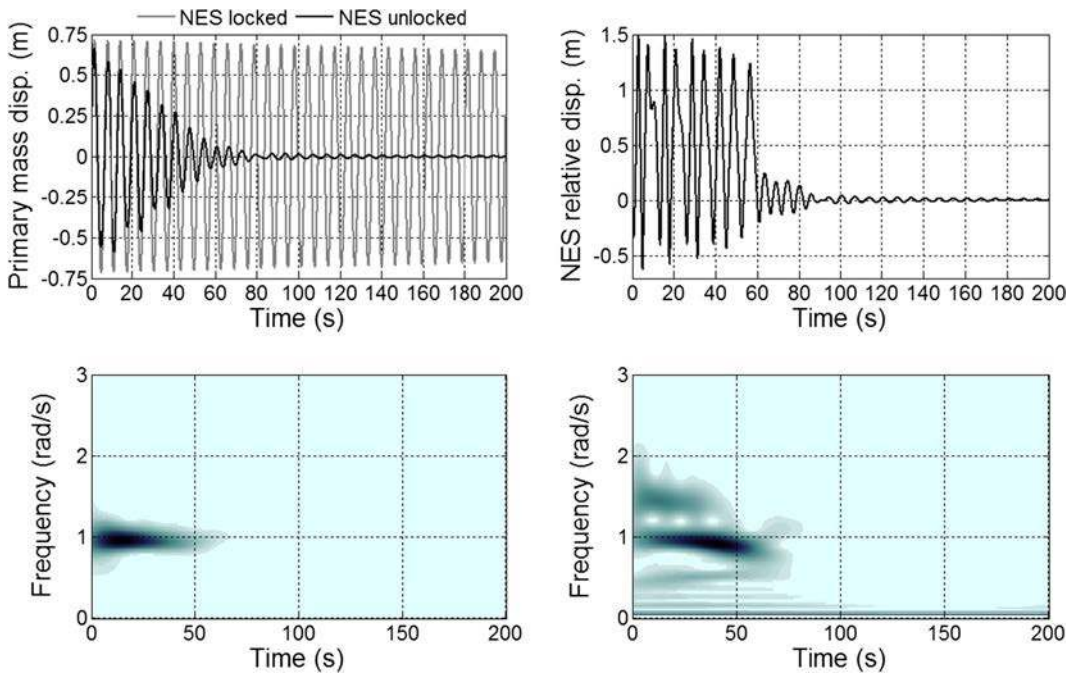

Fig. 12 Time histories of the displacement of the primary mass and the relative displacement of the optimized modified NES mass and their corresponding wavelet transforms for $\dot{x}_2\,(0) = 0.7$ m/s

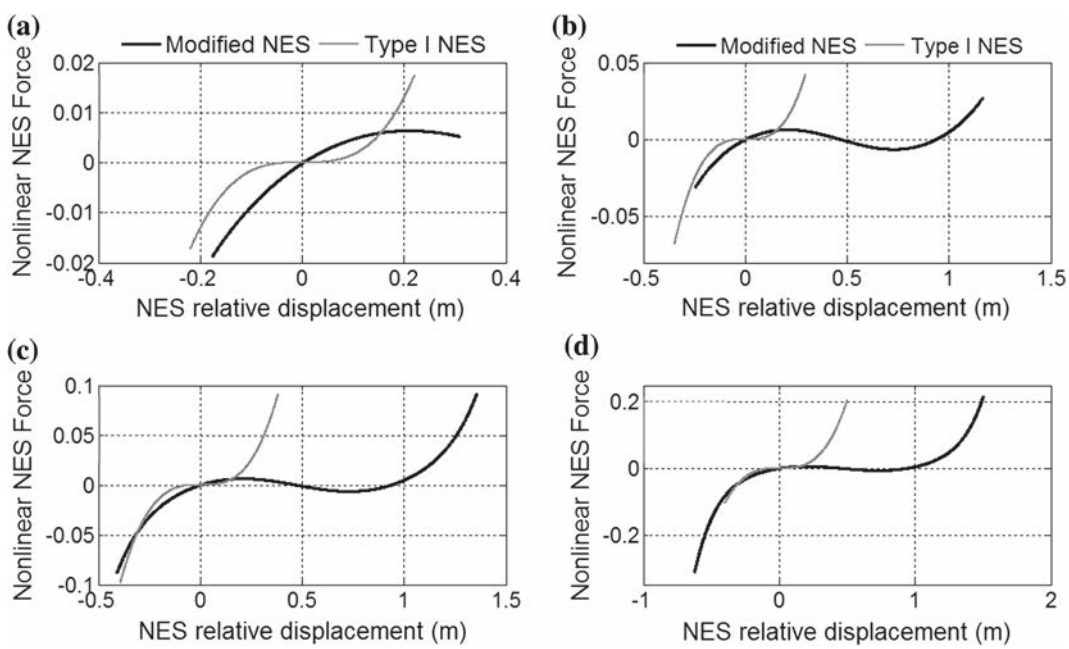

Fig. 13 The actual nonlinear NES force versus the relative displacement of the attached NES mass for **a** $\dot{x}_2\,(0) = 0.1$ m/s, **b** $\dot{x}_2\,(0) = 0.25$ m/s, **c** $\dot{x}_2\,(0) = 0.4$ m/s, and **d** $\dot{x}_2\,(0) = 0.7$ m/s

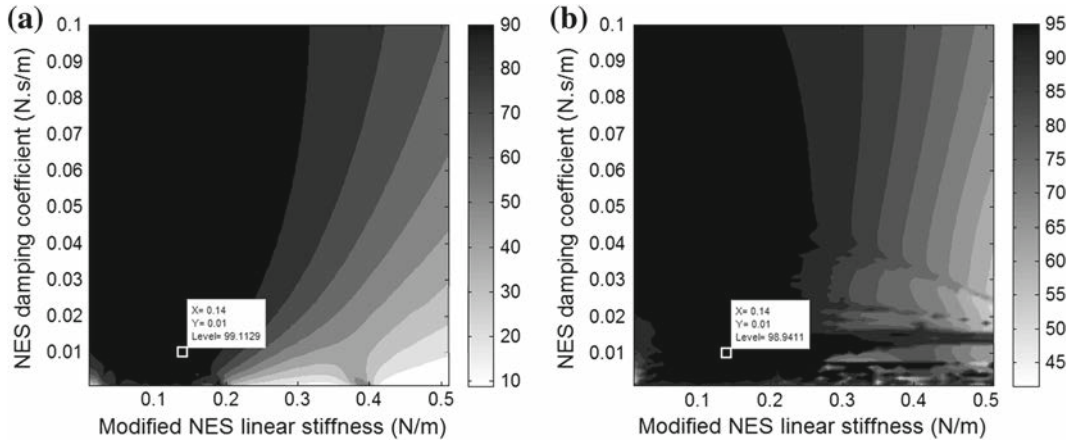

Fig. 14 The effect of the NES damping and the linear stiffness component on the modified NES performance in energy dissipation (*colored bar*) for $\dot{x}_2\,(0) = 0.1$ m/sin (**a**) and $\dot{x}_2\,(0) = 0.4$ m/sin (**b**)

mance of the modified NES is not significantly affected by any significant change in its damping and stiffness. The figure shows that the modified NES is more robust to the change in damping and stiffness than the Type I NES. This is an important advantage to the modified NES for real life applications.

3.2 NES performance under multi input energies

The effect of multi input energies on the performance of the optimized NESs is investigated here. To enrich the comparison, the optimized linear absorber of which $\eta = 99$ % at the damping $\lambda = 0.01$ N s/m and the linear coupling stiffness $k = 0.04$ N/m is also considered. The mass of the linear structure is given an amount of initial input energy at time $t = 0$, and then another amount of external energy is induced at later time $t = t_1$. The ratio of the maximum amplitude in the displacement of the primary mass when the NES (or the linear absorber) is unlocked to the maximum amplitude when the NES (or the linear absorber) is locked is plotted in Fig. 15 for 100 s of simulation at multi input energies. This ratio is shown in Fig. 15a for the modified NES, Fig. 15b for the Type I NES, and Fig. 15c for the linear absorber at the corresponding velocities to the external input energies induced into the linear structure at $t = 0$ and $t = 5$ s. For Fig. 15d–f the external energies are induced into the linear structure at $t = 0$ and $t = 10$ s. This ratio for Type I NES, the modified NES and the linear absorber is found to exceed a unity for very small lesions in the figure. This common dynamic behavior between the considered NESs and the linear absorber can be considered insignificant to affect the overall performance in energy dissipation. Furthermore, the comparison between Fig. 15d of the modified NES and Fig. 15f of the linear absorber shows that the amplitude ratio is less for the system with the modified NES than that with the linear absorber as shown in the colored bar. Hence, the modified NES performs better than the linear absorber under multiple input energies.

3.3 Initially loaded springs

The case for initially loaded springs (compressed or elongated) is investigated here. The system is simulated for the parameters $L = 1$ m, $L_0 = 0.97L$, $k = 0.3$ N/m, $m = 0.05$ kg, $\lambda = 0.016$ N s/m, $M = 1$ kg, $\lambda_p = 0.005$ N s/m, and $k_p = 1$ N/m. At these parameters, we obtain $z_c = 0.243$ m, $k_1 = 0.019$, $k_2 = 0.329$, $k_3 = 0.262$, and $k_4 = 0.232$. The initial velocities and displacements for the simulation are set to, $x_2\,(0) = 0$, $\dot{x}_2\,(0) = v_0$ for $v_0 > 0$, $\dot{x}_1\,(0) = 0$, and $x_1\,(0) = -nz_c$ for $n = 0, 1, 2, 3$, and 4. For $n = 0$ the NES attachment is now positioned at its right stable equilibrium position which coincides with the primary mass equilibrium position, for $n = 1$ the springs of the NES attachment are in their vertical compressed position, for $n = 2$ the NES attachment is positioned at its left stable equilibrium position, and for $n = 3$ and $n = 4$ the NES attachment is positioned away from its left stable equilibrium position where the NES springs are now in tension. The energy pumping

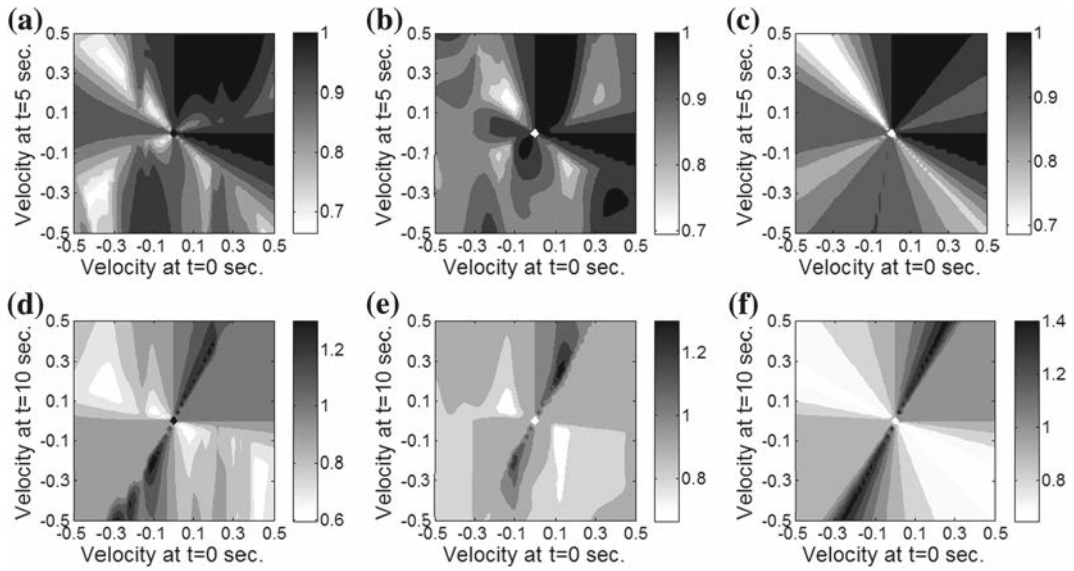

Fig. 15 Amplitude ratio (*colored bar*) under the effect of multi initial energies induced to the linear structures at different times in **a** and **d** for the modified NES; **b, e** for the Type I NES; and **c, f** for the linear absorber

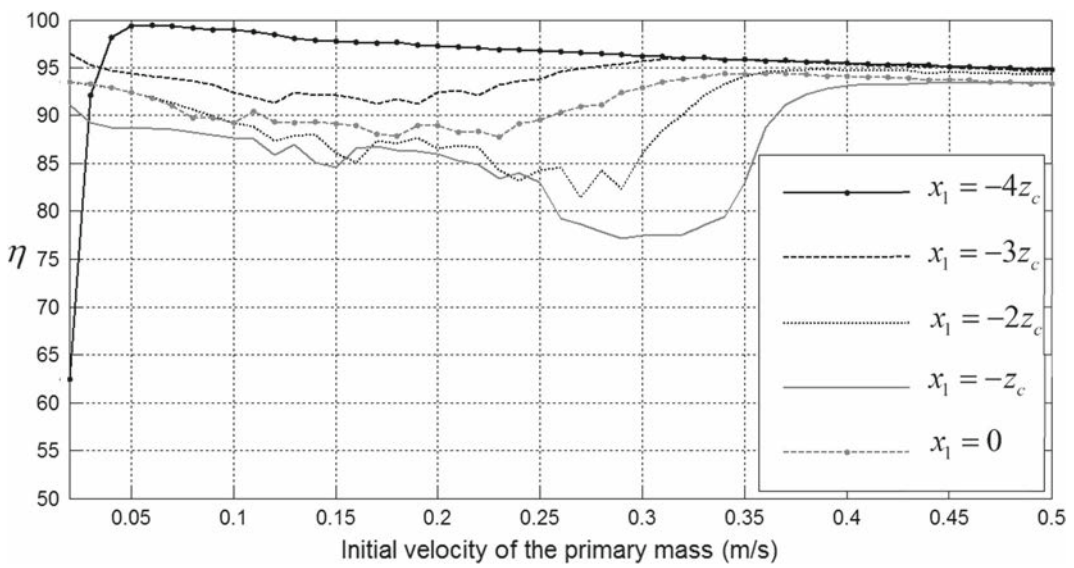

Fig. 16 Percentage of the initial energy induced into primary mass dissipated by the NES for various initial velocities of the primary mass and initial positions of the NES mass

from the primary linear structure to the NES is again quantified by η. The simulation results for various initial velocities of the primary mass and different initial positions of the NES mass are shown in Fig. 16. It is observed in the figure that the modified NES with negative stiffness components still performs much better than Type I NES when its initial position is now at the right equilibrium position ($x_1(0) = 0$) which coincides with primary mass initial position ($x_2(0) = 0$). However, further enhancement in this NES performance is observed when $x_1 = -4z_c$. This interesting finding shows that 99.5 % of the input energy induced into the linear structure is immediately dissipated by the NES when $\dot{x}_2(0) = 0.07$ m/s. To verify this observation,

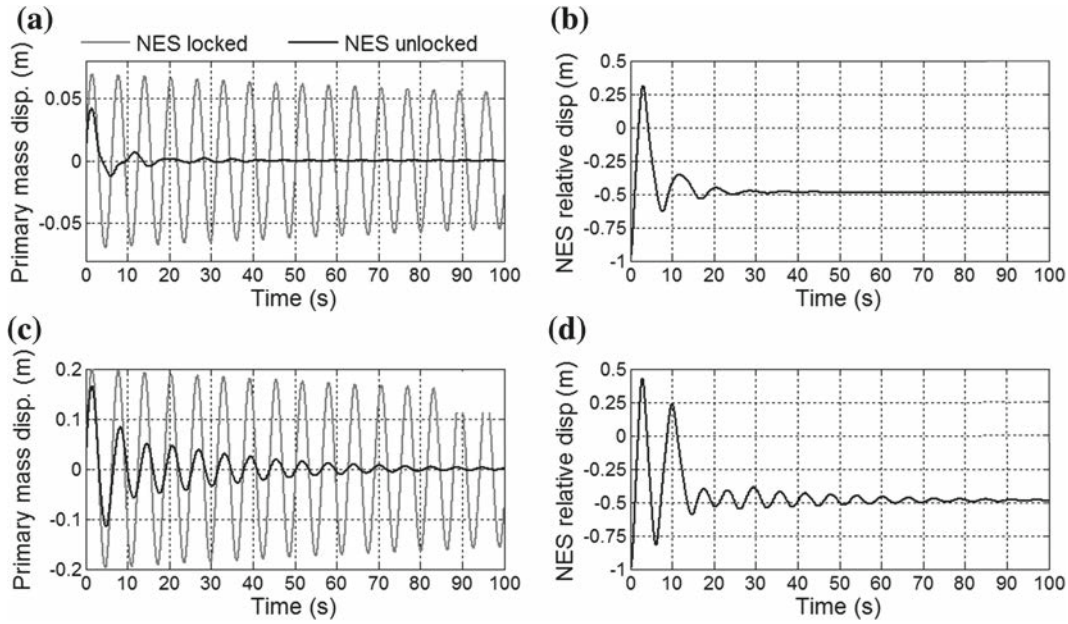

Fig. 17 Time histories of the displacement of the primary mass and the corresponding relative displacement of the NES mass for $\dot{x}_2\,(0) = 0.07$ m/s in **a** and **b** and for $\dot{x}_2\,(0) = 0.2$ m/s in **c** and **d**

the time histories for the primary mass displacement and the NES mass relative displacement are plotted in Fig. 17a and b. The significant reduction in the vibration amplitudes of the primary linear structure is clear in the first cycle of oscillation. This reduction is due to fact that the NES force is dominated by the negative stiffness components which make this force to act in the opposite direction of the motion of the primary mass, even though both of the structure and NES masses are moving in the same direction. Similar observations are obtained for higher velocity of the linear structure as shown in Fig. 17c and d. These considerable enhancements in the NES performance are achieved here by the negative stiffness components. The NES relative displacements in Fig. 17 coincide with the range of the well-approximation of the NES force that previously plotted in Fig. 2b.

4 Two-story physical structure

The modified bistable NES with negative linear and nonlinear stiffness components is investigated here with the physical parameters of the two-degree-of-freedom physical structure in [20]. The physical parameters of this two-story test structure are considered here where they are given in matrix form as

$$M = \begin{bmatrix} 24.3 & 0 \\ 0 & 24.2 \end{bmatrix} \text{kg},$$
$$K = \begin{bmatrix} 15{,}040 & -8{,}220 \\ -8{,}220 & 8{,}220 \end{bmatrix} \text{N/m},$$
$$C = \begin{bmatrix} 1.263 & -0.295 \\ -0.295 & 0.968 \end{bmatrix} \text{N s/m}, \quad (5)$$

where M is the mass matrix, K is the stiffness matrix, and C is the damping matrix. This structure has the natural frequencies $f_1 = 1.69$ Hz and $f_2 = 4.63$ Hz. The Type I NES of mass $m = 2$ kg is coupled to top floor of the structure that has the mass $M_2 = 24.2$ kg. The damping λ and the nonlinear stiffness k_{nl} of the Type I NES are optimized for this structure at equal initial velocities of 0.2 m/s of each floor. Consequently, the optimized physical parameters of Type I NES are $\lambda = 3$ N s/m and $k_{\text{nl}} = 3.2 \times 10^5$ N/m^3. Using the same optimized damping $\lambda = 3$ N s/m of Type I NES, same NES mass of $m = 2$ kg, and the spring unloaded physical length $L = 0.25$ m, the modified NES with negative linear and nonlinear stiffness components is now optimized for L_0 and the linear transverse stiffness$k$as shown in Fig. 18. It is observed that a wide zone of

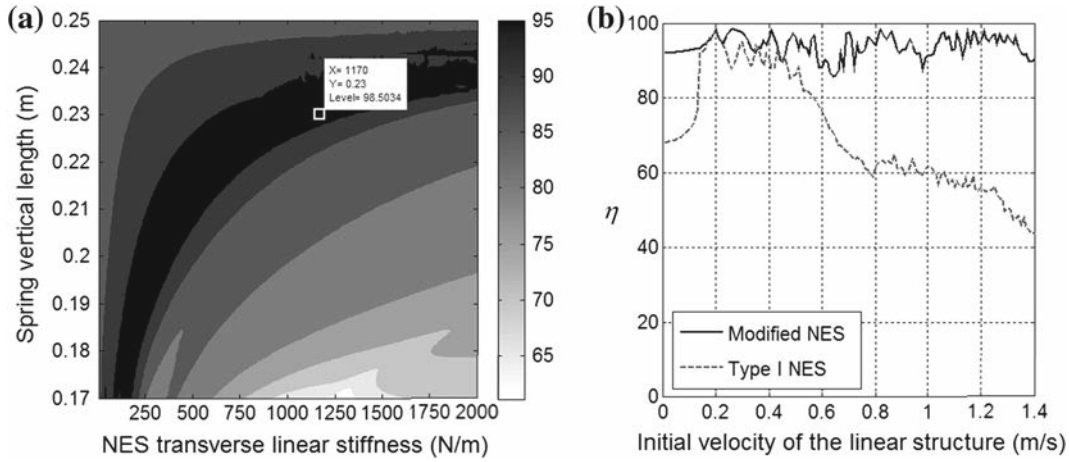

Fig. 18 Percentage of the initial energy induced into the primary structure dissipated by the NES (*colored bar*) for various values of the transverse spring stiffness k and the transverse vertical compressed length L_0 in the modified NES in **a** and the comparison with the optimized Type I NES in **b** for 20 s of simulation

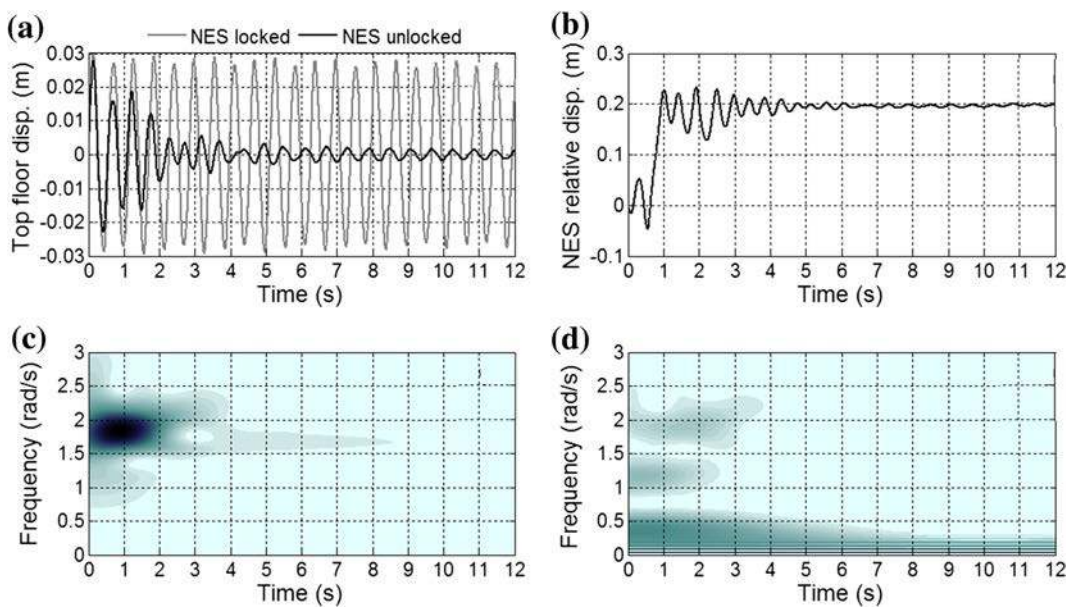

Fig. 19 Time histories of the displacement of the top floor and the relative displacement of the optimized modified NES mass and their corresponding wavelet transforms for $\dot{x}_2\,(0) = 0.27$ m/s

the parameters at which high performance of the modified NES is achieved appears as shown in the figure. For the following analysis, the optimized values of $L_0 = 0.23$ m and $k = 1{,}170$ N/mat which the NES performance reaches $\eta = 98.5$ % are selected. At these values, the performance of the optimized modified NES and the Type I NES is compared for wide range of initial input energies induced into the structure by equal initial velocities at each floor. For 20 s of simulation, the performance of the modified NES is found to be considerably enhanced compared to the Type I NES as shown in Fig. 18b. These observations agree well with those obtained for the previous single-floor linear structure in Fig. 3.

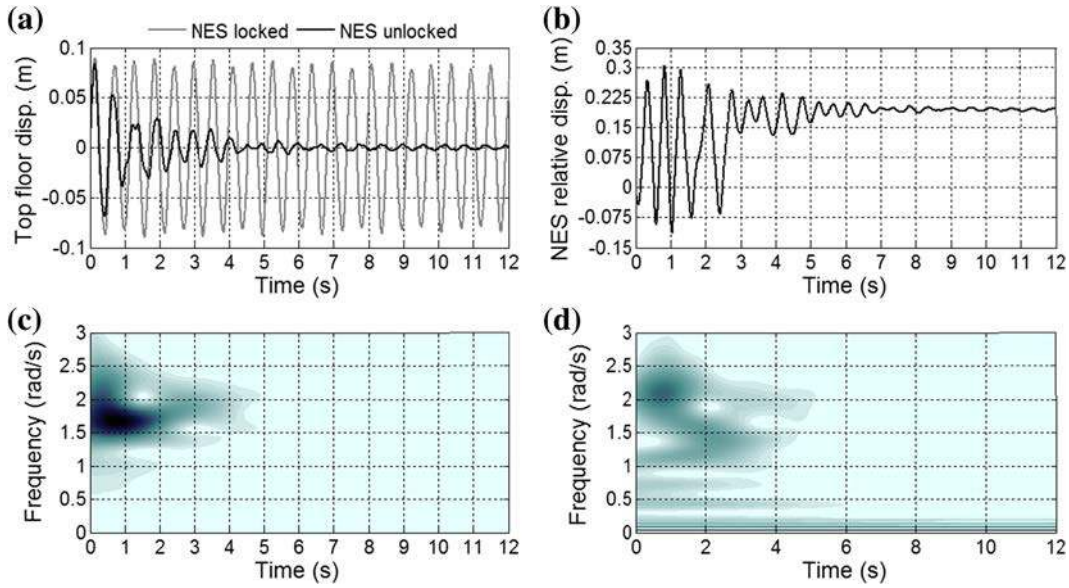

Fig. 20 Time histories of the displacement of the top floor and the relative displacement of the optimized modified NES mass and their corresponding wavelet transforms for $\dot{x}_2\,(0) = 0.82$ m/s

Furthermore, the time histories of the top floor and the NES relative displacements and their corresponding wavelet transforms are shown in Fig. 19 at an intermediate energy corresponding to initial velocity of 0.27 m/s at each floor of the structure. The NES mass performs one full oscillation at its left equilibrium position, and then it jumps to the right equilibrium position to continue oscillation, until it settles there as shown in Fig. 19b. This jump between the equilibrium positions gives the NES mass long stroke of motion in which significant and rapid energy dissipation is achieved. The wavelet transform in Fig. 19c shows the strong immediate resonance capture between the NES mass and the top floor at 1:1 NNM branch near $f_1 = 1.69$ Hz. In addition, the modified NES keeps its strong cascade of resonance captures at 1:1 NNM branch near $f_1 = 1.69$ Hz and the NNM branches of low NNM frequencies as shown in Fig. 19d. This immediate cascade of resonance captures scatters a significant portion of the input energy in a very short time which leads to strong vibration suppression in the structure. Similar observations are obtained for the results in Fig. 20 where the time histories are obtained at high input energy corresponding to initial velocity of 0.82 m/sat each floor of the structure. These observations also agree well with those obtained for the single-floor linear structure considered in Fig. 3.

5 Concluded remarks

Realization of the negative linear and nonlinear stiffness components and their effect on the targeted energy transfer (TET) in the nonlinear energy sinks (NESs) have been addressed here. The linear and nonlinear negative stiffness components in the nonlinear bistable energy sink which are realized here through the modified configuration of the geometric nonlinearity have been found to considerably enhance the NES performance for passive energy pumping and local rapid energy dissipation. Furthermore, by considering the negative stiffness components in the NES with a proper initial position of the NES mass relative to the primary structure mass, the modified NES is found to be able to dissipate 97–99 % of the input energy induced into the linear structure mass for broadband initial energies. This ability for rapid energy transfer and dissipation makes the NES strongly suppress the vibration amplitudes of the linear structure even at the first cycle of oscillation. The high performance of the modified NES with negative stiffness components can be maintained for broadband of initial input energies by an immediate cascade of resonance captures at low and high NNM frequencies. In addition, the modified NES is found to maintain its high performance in shock mitigation for multi external energy inputs at different impulse times.

The findings in this paper are expected to enrich the fields of applications of this modified bistable NES. Finally, this NES can be named as Type VII NES to be distinguished from the other six types of NESs in the literature.

References

1. Vakakis, A.F., Gendelman, O.V., Kerschen, G., Bergman, L.A., McFarland, D.M., Lee, Y.S.: Nonlinear Targeted Energy Transfer in Mechanical and Structural Systems, I and II. Springer, Berlin (2008)
2. Gendelman, O., Manevitch, L.I., Vakakis, A.F., Closkey, R.M.: Energy pumping in nonlinear mechanical oscillators: part I—dynamics of the underlying Hamiltonian systems. J. Appl. Mech. **68**(1), 34–41 (2001)
3. Vakakis, A.F., Gendelman, O.: Energy pumping in nonlinear mechanical oscillators: part II—resonance capture. J. Appl. Mech. **68**(1), 42–48 (2001)
4. Lee, Y.S., Kerschen, G., Vakakis, A.F., Panagopoulos, P., Bergman, L., McFarland, D.M.: Complicated dynamics of a linear oscillator with a light, essentially nonlinear attachment. Phys. D **204**(1–2), 41–69 (2005)
5. Gourdon, E., Alexander, N.A., Taylor, C.A., Lamarque, C.H., Pernot, S.: Nonlinear energy pumping under transient forcing with strongly nonlinear coupling: theoretical and experimental results. J. Sound Vib. **300**, 522–551 (2007)
6. Quinn, D.D., Gendelman, O., Kerschen, G., Sapsis, T.P., Bergman, L.A., Vakakis, A.F.: Efficiency of targeted energy transfers in coupled nonlinear oscillators associated with 1:1 resonance capture: part I. J. Sound Vib. **311**, 1228–1248 (2008)
7. Sapsis, T.P., Vakakis, A.F., Gendelman, O.V., Bergman, L.A., Kerschen, G., Quinn, D.D.: Efficiency of targeted energy transfers in coupled nonlinear oscillators associated with 1:1 resonance captures: part II, analytical study. J. Sound Vib. **325**, 297–320 (2009)
8. McFarland, D.M., Bergman, L.A., Vakakis, A.F.: Experimental study of non-linear energy pumping occurring at a single fast frequency. Int. J. Non-Linear Mech. **40**, 891–899 (2005)
9. AL-Shudeifat, M.A.: Analytical formulas for the energy, velocity and displacement decays of purely nonlinear damped oscillators. J. Vib. Control. doi:10.1177/1077546313493817.
10. Sapsis, T.P., Quinn, D.D., Vakakis, A.F., Bergman, L.A.: Effective stiffening and damping enhancement of structures with strongly nonlinear local attachments. J. Vib. Acoust. **134**, 011016-1 (2012)
11. Vakakis, A.F.: Shock isolation through the use of nonlinear energy sinks. J. Vib. Control **9**, 79–93 (2003)
12. Sigalov, G., Gendelman, O.V., AL-Shudeifat, M.A., Manevitch, L.I., Vakakis, A.F., Bergman, L.A.: Resonance captures and targeted energy transfers in an inertially coupled rotational nonlinear energy sink. Nonlinear Dyn. **69**(4), 1693–1704 (2012)
13. Sigalov, G., Gendelman, O.V., AL-Shudeifat, M., Manevitch, L.I., Vakakis, A.F., Bergman, L.A.: Alternation of regular and chaotic dynamics in a simple two-degree-of-freedom system with nonlinear inertial coupling. Chaos **22**(1), 013118 (2012)
14. Gendelman, O.V., Sigalov, G., Manevitch, L.I., Mane, M., Vakakis, A.F., Bergman, L.A.: Dynamics of an eccentric rotational nonlinear energy sink. J. Appl. Mech. **79**(1), 011012.1–011012.9 (2012)
15. Nucera, F., Vakakis, A.F., McFarland, D.M., Bergman, L.A., Kerschen, G.: Targeted energy transfers in vibro-impact oscillators for seismic mitigation. Nonlinear Dyn. **50**, 651–677 (2007)
16. Karayannis, I., Vakakis, A.F., Georgiades, F.: Vibro-impact attachments as shock absorbers. Proc. IMechE. J. Mech. Eng. Sci. **222**(C), 1899–1908 (2008)
17. Nucera, F., McFarland, D.M., Bergman, L.A., Vakakis, A.F.: Application of broadband nonlinear targeted energy transfers for seismic mitigation of a shear frame: I. Computational results. J. Sound Vib. **329**(15), 2973–2994 (2010)
18. Lee, Y.S., Nucera, F., Vakakis, A.F., McFarland, D.M., Bergman, L.A.: Periodic orbits, damped transitions and targeted energy transfers in oscillators with vibro-impact attachments. Phys. D **238**(18), 1868–1896 (2009)
19. Georgiadis, F., Vakakis, A.F., McFarland, D.M., Bergman, L.A.: Shock isolation through passive energy pumping caused by non-smooth nonlinearities. Int. J. Bifurcat. Chaos **15**(6), 1–13 (2005)
20. AL-Shudeifat, M.A., AL-Shudeifat, M.A., Wierschem, N., Quinn, D.D., Vakakis, A.F., Bergman, L.A., Spencer Jr, B.F.: Numerical and experimental investigation of a highly effective single-sided vibro-impact nonlinear energy sink for shock mitigation. Int. J. Non-Linear Mech. **52**, 96–109 (2013)
21. Wierschem, N., Luo, J., Hubbard, S., Fahnestock, L., Spencer, Jr, B., Vakakis, A., Bergman, L.: Experimental testing of a large 9-story structure equipped with multiple nonlinear energy sinks subjected to an impulsive loading. Structures congress, pp. 2241–2252 (2013).
22. Quinn, D.D., Wierschem, N., Hubbard, S., AL-Shudeifat, M.A., Ott, R.J., McFarland, D.M., Vakakis, A.F., Bergman, L.A.: Equivalent modal damping, stiffening and energy exchanges in multi-degree-of-freedom systems with strongly nonlinear attachments. J. Multi-Body Dyn. **226**(2), 122–146 (2012)
23. Wierschem, N., Quinn, D.D., Hubbard, S., AL-Shudeifat, M.A., McFarland, M., Luo, J., Fahnestock, L.A., Spencer Jr, B.F., Vakakis, A.F., Bergman, L.A.: Passive damping enhancement of a two-degree-of-freedom system through a strongly nonlinear two-degree-of-freedom attachment. J. Sound Vib. **331**(25), 5393–5407 (2012)
24. Jiang, X., McFarland, D.M., Vakakis, A.F.: Steady state passive nonlinear energy pumping in coupled oscillators: theoretical and experimental results. Nonlinear Dyn. **33**, 87–102 (2003)
25. Malatkar, P., Nayfeh, A.H.: Steady-state dynamics of a linear structure weakly coupled to an essentially nonlinear oscillator. Nonlinear Dyn. **47**, 167–179 (2007)